JTTEE5 5:283-288

Characterization of Plasma Sprayed Fe-17Cr-38Mo-4C Amorphous Coatings Crystallizing at Extremely High Temperature

K. Kishitake, H. Era, and F. Otsubo

A Fe-17Cr-38Mo-4C alloy powder was plasma sprayed by three processes: an 80 kW low-pressure plasma spray (LPPS), a 250 kW high-energy plasma spray (HPS), and a 40 kW conventional plasma spray (APS). The as-sprayed coating obtained by the LPPS process is composed of only amorphous phase. As-sprayed coatings obtained by the HPS and APS processes are a mixture of amorphous and crystalline phases. The three as-sprayed coatings exhibit a high hardness of 1000 to 1100 DPN. The amorphous phase in these coatings crystallizes at a high temperature of about 920 K. A very fine structure composed of hard χ-phase and carbides is formed after crystallization. The hardness of the coating obtained by LPPS reaches a maximum of 1450 DPN just after crystallization on tempering and retains a high hardness more than 1300 DPN after tempering at high temperatures of 1173 or 1273 K. The corrosion potential of the amorphous coating is the highest among the three coatings and higher than that of a SUS316L stainless steel coating. The anodic polarization measurements infer that the corrosion resistance of the amorphous coating is superior or comparable to SUS316L stainless steel coating in H_2SO_4 solution.

Keywords amorphous, corrosion resistance, crystallization, iron alloy, plasma spraying

1. Introduction

NONEQUILIBRIUM phases in rapidly solidified high-carbon iron alloys have been investigated to develop thermal spray materials for wear resistance. The nonequilibrium phases, such as amorphous phase (Ref 1, 2), ψ-phase (Ref 3, 4), χ-phase (Ref 5, 6), ε-phase (Ref 7, 8), and γ-phase (Ref 9, 10) arise in rapidly solidified high-carbon iron alloys. A large amount of fine carbides are formed in the alloys by the decomposition of these nonequilibrium phases and bring about a very high hardness (Ref 2, 11, 12). The high-carbon iron alloys, composed of amorphous phase or a mixture of nonequilibrium ε- and γ-phases, have been plasma sprayed for wear-resistant applications. These coatings retain a very high hardness up to 1000 K, and the corrosion resistance of amorphous coatings is superior to SUS316L stainless steel coating in H_2SO_4 solution (Ref 13-15). Also, the alloy powders, forming nonequilibrium phases through rapid solidification, have been used as thermal spray materials for wear resistance at high temperatures (Ref 16).

On the basis of prior work, it is expected that an amorphous phase having a high decomposition temperature is available for wear and corrosion resistance up to the crystallizing temperature. The present work was carried out to obtain amorphous coatings of a high-carbon iron alloy having a composition similar to the iron-base amorphous alloy crystallizing at an extremely high temperature reported by Inoue et al. (Ref 17). Three plasma spraying methods were performed, and characterization and the tempering behavior of the coatings were investigated.

K. Kishitake, H. Era, and **F. Otsubo,** Department of Materials Science and Engineering, Faculty of Engineering, Kyushu Institute of Technology, Kita-Kyushu 804, Japan.

2. Experimental Procedure

The iron alloy powder was produced by gas atomization after melting electrolytic iron, graphite, and ferroalloys using an induction furnace. The chemical composition of the alloy powder (in wt%) is 16.9 Cr, 37.9 Mo, 3.95 C, 0.84 Si, bal Fe. A small amount of silicon is added to prevent oxidation during atomization. Alloy powders smaller than 45 μm diameter were used for spraying in this study. The coatings were sprayed onto mild steel by 80 kW low-pressure plasma spraying (LPPS), 250 kW high-energy plasma spraying (HPS), and 40 kW conventional plasma spraying (APS) under the conditions shown in Table 1. The coating thickness was 100 μm only for the LPPS process and about 500 μm for the other

Table 1 Plasma spraying conditions

LPPS	
Atmosphere	In chamber at 6500 Pa
Current, A	1200
Voltage, V	60
Spray distance, mm	300
HPS	
Atmosphere	In the air
Current, A	450
Voltage, V	430
Spray distance, mm	200
APS	
Atmosphere	In the air
Current, A	30
Voltage, V	600
Spray distance, mm	100

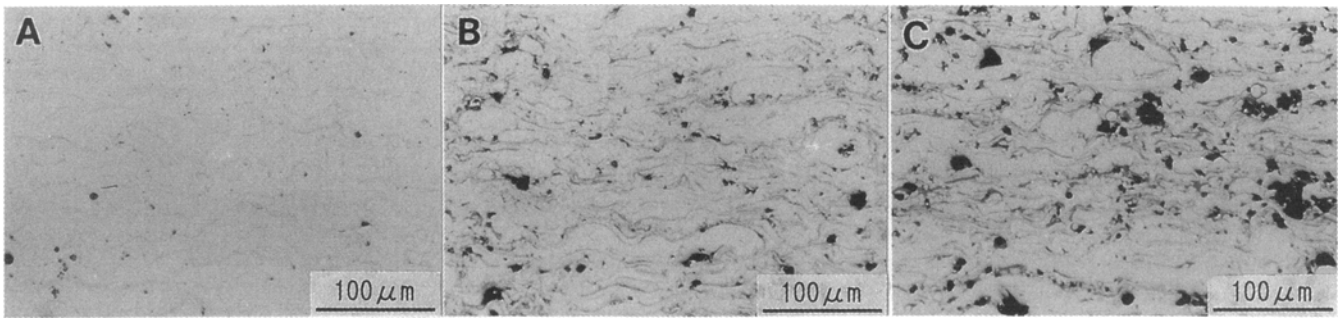

Fig. 1 Optical micrographs of as-sprayed coatings. (a) LPPS. (b) HPS. (c) APS

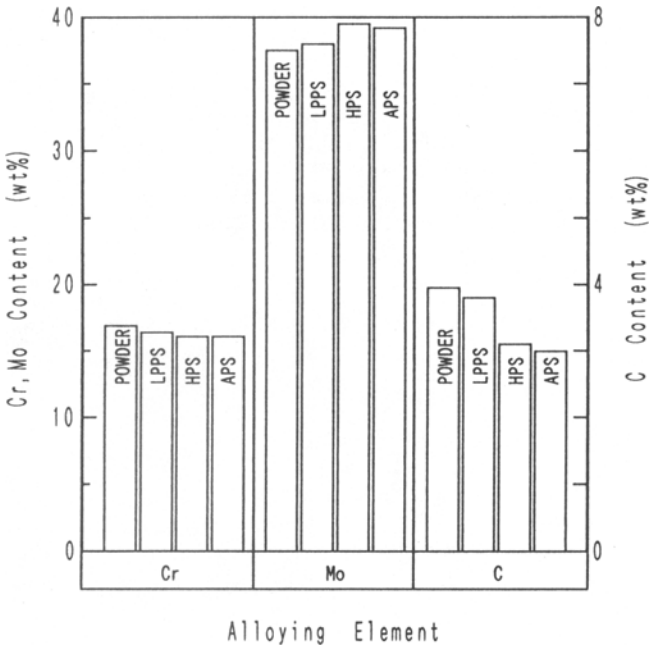

Fig. 2 Change in content of alloying element by plasma spraying

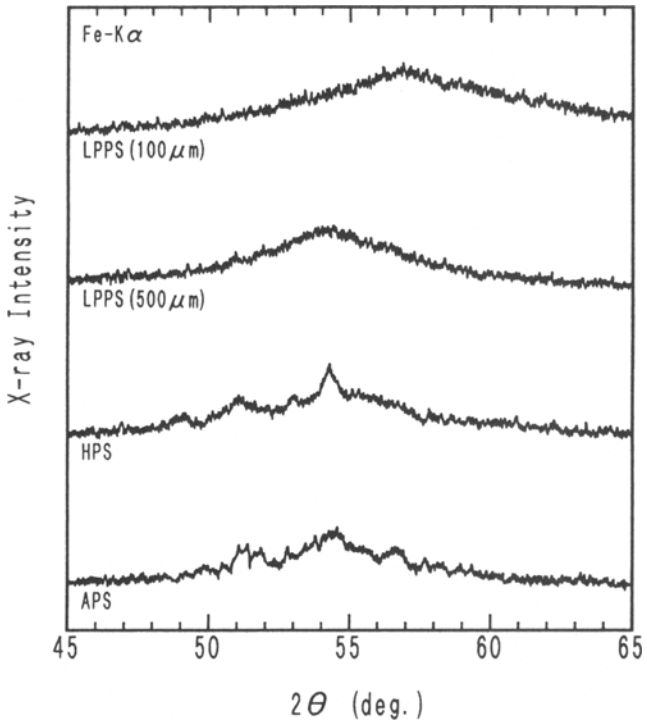

Fig. 3 X-ray diffraction patterns of as-sprayed coatings

three processes. The coatings were heated in vacuum at various temperatures up to 1273 K for 1 h.

The characteristics of the coatings were investigated by means of x-ray diffraction (XRD) (Fe-Kα radiation), microhardness test (30 tests per specimen with a 50 g load), optical microscopy, scanning electron microscopy (SEM), and transmission electron microscopy (TEM). Also, the macroscopic crystallization behavior of the amorphous phase in the coatings was examined by means of differential thermal analysis (DTA) at a heating rate of 20 K/min.

The coatings were also evaluated from the anodic polarization curves using a potentiostat. Prior to the electrochemical measurement, the coatings were polished with an alumina powder up to 0.05 μm and were masked with an acid-resistant lacquer to form an area of 1 cm^2. The electrolyte used was deaerated 1*N* H_2SO_4 solution at 303 K, and the opposite electrode and reference electrode used were platinum and a saturated calomel electrode (SCE), respectively. The electrochemical measurement of the coatings was carried out by scanning the corrosion potential to +1.1 V (versus SCE) at a scanning rate of 60 mV/min after stabilization at –0.7 V (versus SCE) for 10 min.

3. Results and Discussion

3.1 *Structure of As-Sprayed Coatings*

Figure 1 shows the optical micrographs of the as-sprayed coatings. Very thin oxide films can be seen; however, few pores are visible in the LPPS coatings. Some pores and oxide films are included in the coatings obtained by HPS, and significant pores and oxide films exist in the APS coatings.

Chemical analysis of the coatings was carried out to investigate the change in chemical composition for the three kinds of plasma spraying processes (Fig. 2). The chemical composition of the LPPS coating was not different from the feedstock powder. The carbon content of the coatings by HPS and APS proc-

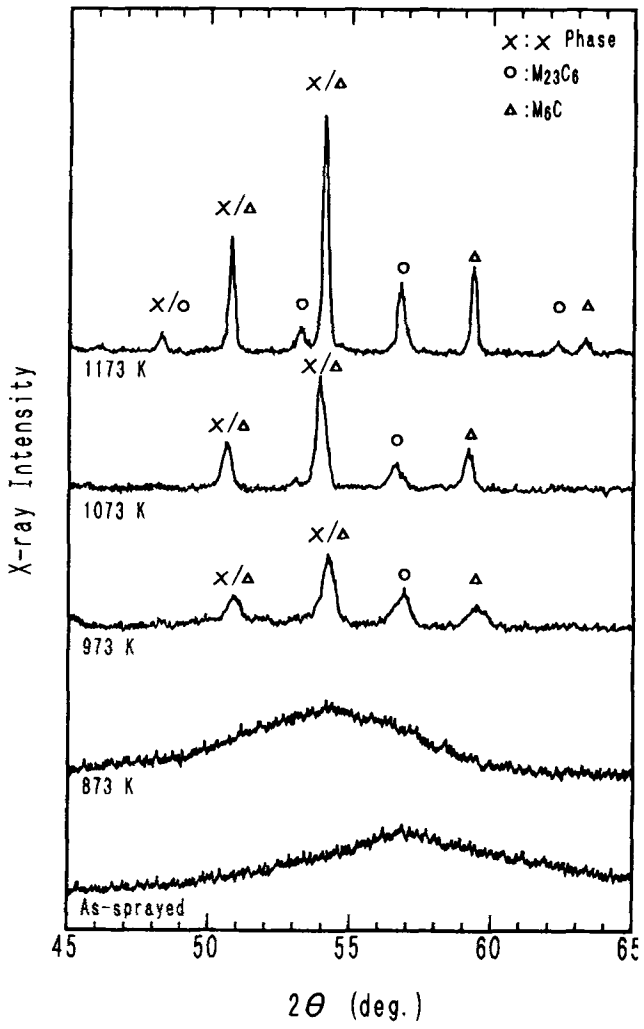

Fig. 4 X-ray diffraction patterns of coatings tempered at various temperatures

esses decreased considerably, and the molybdenum content increased slightly as the result of the carbon decrease.

Figure 3 shows XRD patterns of the as-sprayed coatings. Only a broad peak, i.e., a halo pattern, appears for the coatings obtained by LPPS. It is noted that the peak position of the halo patterns is different between the 100 μm thick and the 500 μm thick coatings. On the other hand, some broad diffraction peaks attributed to crystalline phases arise in addition to a halo pattern for the coatings obtained by the HPS and APS processes. It is seen that an amorphous coating is formed by the LPPS process and a mixture of amorphous and crystalline phases by HPS and APS processes. This may result from the difference of the cooling rate and carbon content in the coatings between the LPPS process and the other processes.

3.2 *Decomposition of Amorphous Phase on Tempering*

X-ray diffraction was carried out to investigate the crystallization of the amorphous coatings after heat treatment at different temperatures for 1 h. Figure 4 shows the XRD patterns of the

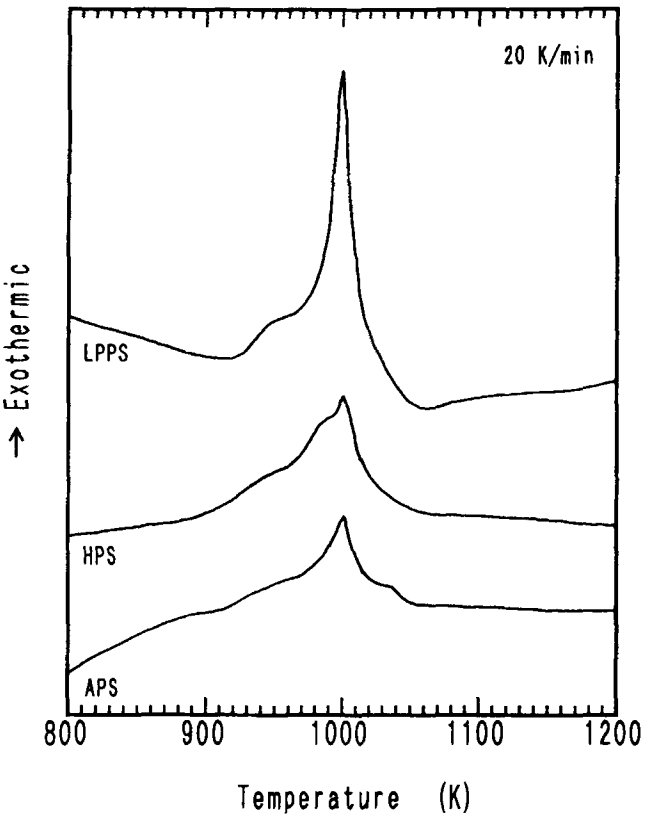

Fig. 5 DTA curves of coatings

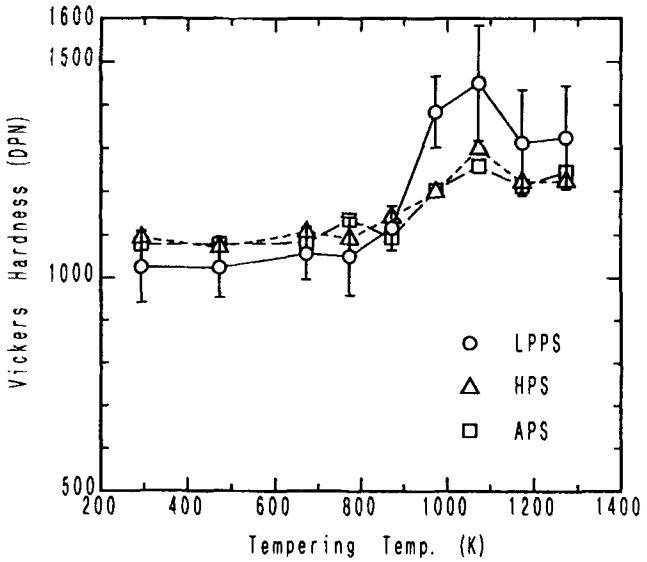

Fig. 6 Change in hardness as a function of tempering temperature. Longitudinal bars at open circles show standard deviation of LPPS coating.

100 μm thick coating obtained by the LPPS process. It is seen that the amorphous phase is retained on tempering up to 873 K, and the peak position of the halo pattern shifts from 57 to 54°. This change of the halo pattern also occurred on tempering at 473 K.

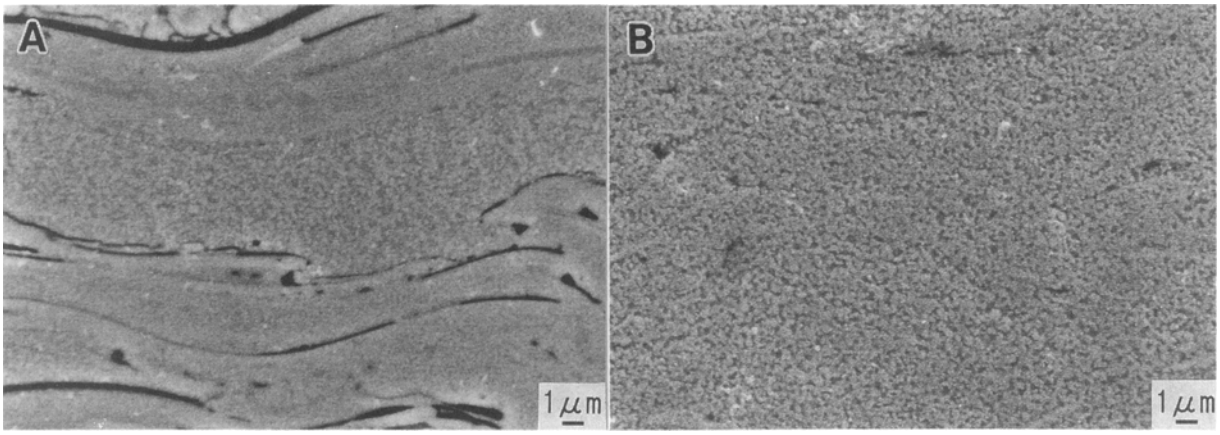

Fig. 7 SEM images of coatings by LPPS process tempered at (a) 1073 K and (b) 1273 K

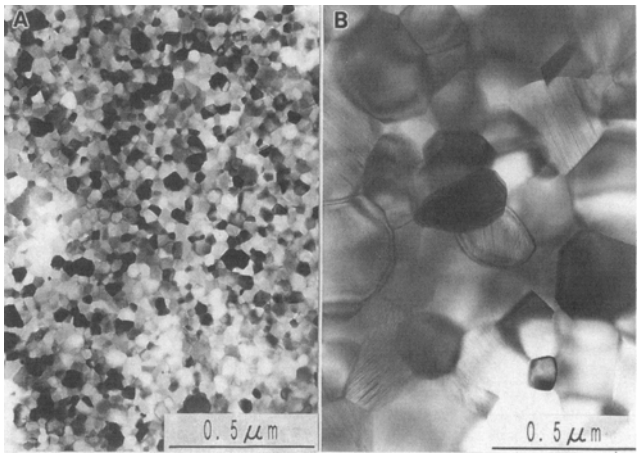

Fig. 8 Bright field images of coatings by LPPS process tempered at (a) 1073 K and (b) 1273 K

The halo pattern of the LPPS coating tempered at 873 K is very similar to that of the 500 μm thick as-sprayed coating shown in Fig. 3. It seems that the atomic configuration was changed by tempering in excess of 473 K. The amorphous structure of the 500 μm thick LPPS as-sprayed coating exhibited a halo pattern centered on 54° may arise from heating induced during thermal spraying. On tempering at 973 K, the amorphous phase crystallizes and the diffraction peaks of χ-phase, $M_{23}C_6$, and M_6C carbides appear. On tempering at 1073 and 1173 K, these peaks become sharp. The amorphous phase in the HPS and APS coatings also crystallizes at 973 K and forms a mixture of χ-phase, $M_{23}C_6$ and M_6C carbides.

Figure 5 shows DTA curves of the coatings. The exothermic peaks attributed to crystallization of the amorphous phases are seen in the range of about 920 to 1050 K. The exothermic peaks of HPS and APS are low compared with that of the LPPS coating because of a smaller volume fraction of the amorphous phase. The amorphous phase in the coatings crystallizes at a temperature of 920 K. This temperature is higher by about 160 K than that of the amorphous phase of the Fe-Cr-Mo-C alloy coating (Ref 15).

3.3 *Hardness*

Figure 6 shows the effect of tempering on coating hardness. All the as-sprayed coatings exhibit a very high hardness of 1000 to 1100 DPN. The hardness is not changed significantly by tempering up to 873 K. The coating hardnesses begin to rise on tempering at 973 K because of crystallization of amorphous phase, then reached a maximum hardness of 1200 to 1400 DPN when tempered at 1073 K. The hardness of the LPPS coating is higher than the HPS and APS coatings over the crystallization temperature. The difference is mainly attributable to the difference of a volume fraction of the amorphous phase and carbon content in the as-sprayed coatings. The hardness decreases on tempering over 1100 K and reaches 1200 to 1300 DPN after being tempered at 1173 and 1273 K.

Scanning electron micrographs of the LPPS coating tempered at 1073 and 1273 K are shown in Fig. 7(a) and (b), respectively. The coating showing a peak hardness of 1450 DPN reveals a fine structure of χ-phase, $M_{23}C_6$ and M_6C. The coating tempered at 1273 K reveals a coarsened structure compared with the structure showing the peak hardness. Figure 8 shows TEM bright field images of the LPPS coatings tempered at 1073 K (Fig. 8a) and 1273 K (Fig. 8b). Fine equiaxed grains smaller than 0.1 μm in diameter are seen in the coating tempered at 1073 K, as also exhibited by the coating tempered at 1273 K. This nanostructure is formed by crystallization and remains after tempering at 1273 K. Consequently, this amorphous coating exhibits a high hardness at high temperature due to high crystallization temperature and formation of a nanostructure composed of hard χ-phase and carbides at high temperature. It is expected that the amorphous coating is suitable as a wear-resistant coating at high temperature.

3.4 *Electrochemical Properties*

Anodic polarization curves of the as-sprayed and tempered coatings were measured in deaerated 1*N* H_2SO_4 solution at 303 K (Fig. 9). The 18-8 stainless steel (JIS-SUS316L) coating is also shown for comparison purposes. The anodic polarization curves of all the coatings exhibit an activation-passivation transition. The corrosion potential of the LPPS coatings is the highest of these coatings. The difference of corrosion potential

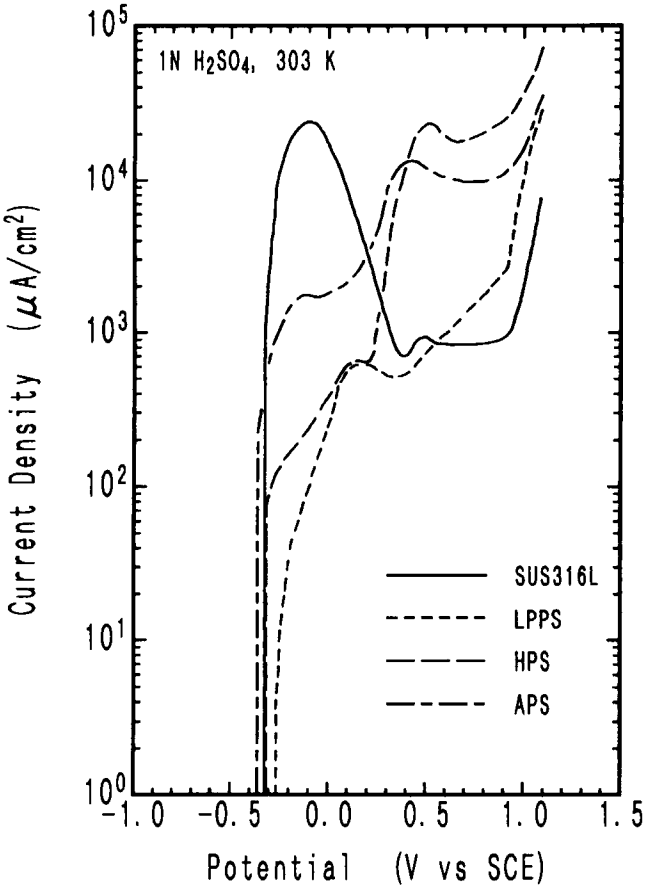

Fig. 9 Anodic polarization curves of as-sprayed coatings

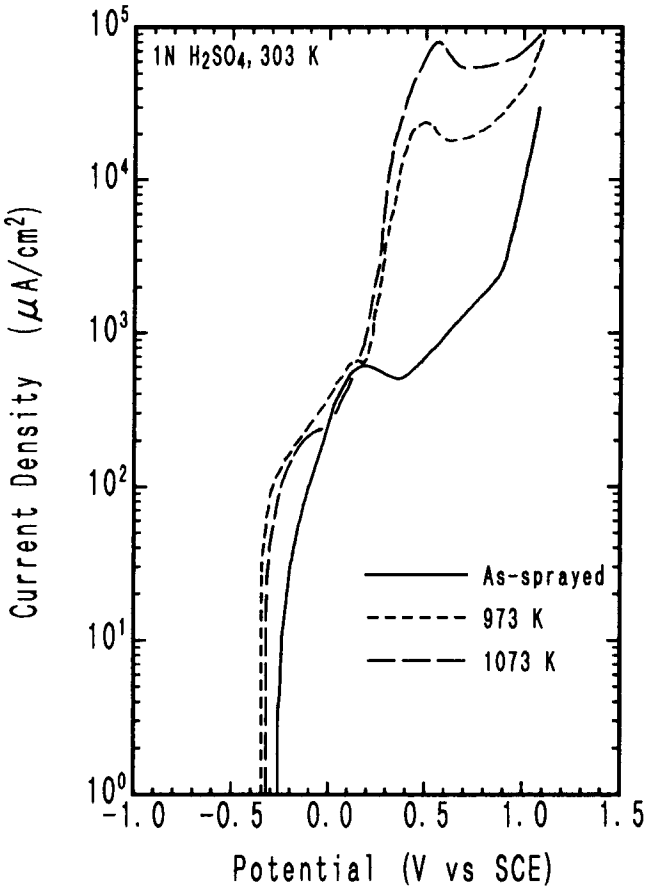

Fig. 10 Anodic polarization curves of coatings obtained by LPPS

among LPPS, HPS, and APS coatings may be attributable to the presence of crystal phases and the occurrence of oxide films in the coatings. The current density of the LPPS coating is the lowest of the three coatings in the measured potential range. Therefore, the corrosion resistance of the LPPS coating is the best of the three coatings. When compared with the SUS316L stainless steel coating, the LPPS coating exhibits higher corrosion potential and lower passivation current density in the active state. In the passive state, the current density of SUS316L stainless steel coating is unchanged, but that of the LPPS coating increases with increasing potential. Accordingly, the LPPS coating is readily passivated, but its passive state is unstable compared with the SUS316L stainless steel coating.

Figure 10 shows the anodic polarization curves of the LPPS coating in H_2SO_4 solution before and after crystallization. The crystallized coatings reveal a low corrosion potential and high current densities compared with the as-sprayed amorphous coating. This deterioration of the corrosion resistance may be attributable to the existence of crystals as second phases.

4. Conclusions

Alloy powders of Fe-17Cr-38Mo-4C were plasma sprayed by 80 kW low-pressure plasma spraying, 250 kW high-energy plasma spraying, and 40 kW conventional plasma spraying. The tempering behavior and electrochemical character of the coatings were investigated. The results obtained are summarized as follows:

- An amorphous coating is obtained by the LPPS process and a mixture of amorphous and crystalline phases is formed by the HPS and APS processes. The as-sprayed coatings show a high hardness of over 1000 DPN.
- The amorphous phase in the coating crystallizes at about 920 K. The coating obtained by the LPPS process shows a hardness of 1450 DPN just after crystallization and retinas a hardness >1300 DPN after tempering at 1273 K. This high hardness is attributable to a very fine structure composed of hard χ-phase and carbides.
- The corrosion resistance of the as-sprayed amorphous coating obtained by LPPS is the best of the three coatings and superior or comparable to the SUS316L stainless steel coating. The amorphous coating is easily passivated, but the passive state is unstable compared with SUS316L stainless steel coating in H_2SO_4 solution.

This amorphous coating is expected to have good wear resistance and corrosion resistance up to the crystallization temperature of 920 K.

Acknowledgments

This work was supported by a Grant-in-Aid of the Ministry of Education in Japan. The authors wish to acknowledge the Plant and Machinery Division of the Nippon Steel Corporation for preparing samples and Mr. K. Nakashima and Mr. T. Kichise, formerly students of Kyushu Inst. of Tech., for experimental assistance.

References

1. A. Inoue and T. Masumoto, Crystallization Behavior of Amorphous High-Carbon Alloy Steels, *Sci. Rep. Research Inst. Tohoku Univ.*, Vol A27, 1979, p 147-158
2. K. Kishitake, H. Era, and F. Otsubo, Enhancement of Hardness by Heat Treatment in Rapidly Solidified High-Carbon Iron Alloys, *Scr. Met. Mater.*, Vol 24, 1990, p 1269-1273
3. H. Era, K. Kishitake, F. Otsubo, and E. Tanaka, A13-Type Phase Revealed in Rapidly Solidified High-Carbon Iron Alloy, *Metall. Trans. A*, Vol 22A, 1991, p 251-253
4. H. Era, K Kishitake, and P. Li, Structure and Decomposition of A13-Type Phase in Rapidly Solidified High-Carbon Cr-Si Iron Alloy, *Metall. Trans. A*, Vol 24A, 1993, p 751-756
5. T. Iwadachi, A. Inoue, T. Minemura, and T. Masumoto, Nonequilibrium Phases in Fe-X-C (X = Cr, Mo, W) Ternary Alloys Quenched Rapidly from Melts, *J. Jpn. Inst. Met.*, Vol 44, 1980, p 245-254 (in Japanese)
6. A. Inoue, L Arnberg, M. Oguchi, U. Backmark, and N. Bäckström, and T. Masumoto, Preparation of Fe-Cr-Mo-C Amorphous Powders and Microstructure and Mechanical Properties of their Hot-Pressed Products, *Mater. Sci. Eng.*, Vol 95, 1987, p 101-114
7. R.C Ruhl and M Cohen, Splat Quenching of Iron-Carbon Alloys, *Trans. AIME*, Vol 245, 1969, p 241-251
8. K. Kishitake, H. Era, F. Otsubo, and E. Tanaka, Nonequilibrium Austenite/ε-Phase Eutectic Revealed in Rapidly Solidified High-Carbon Iron Alloy, *Metall. Trans. A*, Vol 22A, 1991, p 791-792
9. T. Minemura, A. Inoue, and T. Masumoto, Metastable Austenite Phase in Rapidly Quenched Fe-Cr-C Alloys, *Trans. ISIJ*, Vol 21, 1981, p 649-655
10. T. Minemura, A. Inoue, Y. Kojima, and T. Masumoto, Microstructure and Mechanical Properties of Nonequilibrium Austenite in Fe-C-(Mo,W) Systems Rapidly Quenched from Melts, *Trans. ISIJ*, Vol 22, 1982, p 934-941
11. K. Kishitake, H. Era, and F. Otsubo, Structures and Tempering Behavior of Rapidly Solidified High-Carbon Iron Alloys, *Metall. Trans. A*, Vol 22A, 1991, p 775-782
12. K. Kishitake, H. Era, F. Otsubo, P. Li, and N. Wakayama, Tempering Behavior of Rapidly Solidified Eutectic High-Carbon Fe-Cr-Mo-B Alloys, *J. Jpn. Foundry. Soc.*, Vol 65, 1993, p 468-473 (in Japanese)
13. H. Matsumoto, K. Kishitake, T. Irisawa, and H. Era, Characteristics of Rapidly Solidified Coatings Obtained by Thermal Spraying of White Cast Irons, *J. Jpn. Foundry. Soc.*, Vol 62, 1990, p 37-42 (in Japanese)
14. K. Kishitake, H. Matsumoto, H. Era, and T. Irisawa, Characteristics of Rapidly Solidified Coatings Obtained by Thermal Spraying of White Cast Irons Containing Carbide Former Elements, *J. Jpn. Foundry. Soc.*, Vol 62, 1990, p 185-190 (in Japanese)
15. K. Kishitake, H. Era, and F. Otsubo, Formation and Properties of Iron Base Amorphous Coatings by Low Pressure Plasma Spraying, *J. Jpn. Therm. Spray. Soc.*, Vol 32, 1994, p 15-21 (in Japanese)
16. H. Matsumoto and K. Kishitake, "Thermal Sprayed Coating of High-Carbon Iron Alloy," Japanese patent 6-65747, 1994, (in Japanese)
17. A. Inoue, T. Masumoto, S. Arakawa, and T. Iwadachi, Amorphous High-Carbon Alloy Steels Rapidly Quenched from Melts, *Mater. Trans. JIM*, Vol 19, 1978, p 303-304